CROSS-SECTIONAL MICROSTRUCTURAL HOMOGENEITY CHARACTERISTICS ON FATIGUE PERFORMANCE OF STRUCTURAL STEELS IN AIR AND HYDROGEN ENVIRONMENTS *

Douglas Glenn Stalheim[1]
Andrew Slifka[2]
Pello Uranga[3]
Dong-Hoon Kang[4]
Enrico Lucon[5]

Abstract
Structural steel final mechanical properties of strength and ductility are predominately generated by the final ferrite grain size/packet size and homogeneity of that ferrite grain size/packet size through the cross-sectional area. Forty to seventy percent of the strength components come from how fine the final cross-sectional ferrite grain size/packet size that can be produced.[1] All the ductility properties of structural steels for a given microstructure are predominately driven by how fine ***AND*** homogenous the final cross-sectional ferrite grain size/packet size can be refined.[2,3,4] One key ductility property of structural steels used in construction and energy transmission applications is fatigue. Both low and high cycle fatigue can be realized in these end applications, however, low cycle fatigue is typically the predominate mechanism. In construction applications the environment for fatigue is typically air, such as in wind towers or high-rise building construction. In energy applications, there is an interest in high pressure (5.5 – 21 MPa, 800-3000 psi) gaseous hydrogen as an alternative fuel source to fossil fuels. A project to study the effect of the cross-sectional grain size/homogeneity of a relatively pure polygonal ferrite microstructure on the fatigue performance in air and high-pressure gaseous hydrogen has been developed. This paper will discuss the project strategy, microstructure developed for the project and initial test results.

Keywords: Grain Size; Homogeneity; Fatigue; Hydrogen

[1] *Bachelor of Science in Metallurgical Engineering, President, DGS Metallurgical Solutions, Inc., Vancouver, WA, USA.*
[2] *PhD in Materials Science, Materials Research Engineer, Applied Chemicals and Materials Division, National Institute of Standards and Technology (NIST), Boulder, Colorado, USA.*
[3] *PhD in Materials Engineering, Associate Director of Division, Materials and Manufacturing Division, CEIT and University of Navarra, Donostia-San Sebastian, Basque Country, Spain.*
[4] *Master in Materials Science, Research Engineer, Heavy Plate Development Team, Hyundai Steel Technical Research Center, Dangjin, Chungnam, Republic of Korea.*
[5] *PhD in Nuclear Engineering, Mechanical Engineer, Applied Chemicals and Materials Division, National Institute of Standards and Technology (NIST), Boulder, Colorado, USA.*

1 INTRODUCTION

Many structures are designed primarily from the standpoint of fatigue, such as pipelines, support towers, and bridges. Most codes that provide for proper design of structures that are susceptible to fatigue, such as the ASME B31.12 code for Hydrogen Piping and Pipelines base the designs on the strength of the materials [5]. However, strength is not the only consideration in the fatigue resistance of a material, particularly for structural steels, and many structural applications result in loading conditions where fatigue resistance is more important than strength. The mechanical properties of a steel come from microstructure and chemistry, and microstructure is developed from processing. Therefore, fatigue resistance of steels is developed from processing and intimately tied to cross-sectional microstructure.

Various structural steel microstructures primarily related to API grade pipeline steels have been fatigue tested and published in both hydrogen and air over the past 10 years by NIST and other US National Laboratories. NIST has developed a unique multi specimen fatigue testing device with capability for both air and high-pressure gaseous hydrogen atmospheres hence allowing for capabilities to significantly increase productivity of the fatigue test [6]. One of the microstructures fatigue-tested by NIST and Sandia National Laboratories is a production-produced API X60 HIC Sour Service plate grade consisting of a predominately pure microstructure of polygonal ferrite with a low carbon (0.03%), higher Nb content (0.085%) allowing for higher temperature processing (HTP). This was identified as “Alloy D” in the fracture and fatigue testing done in high pressure gaseous hydrogen. This microstructure has performed well in both 800 and 3000 psi hydrogen pressure fracture and fatigue testing, Figure 1 [7,8,9,10,11].

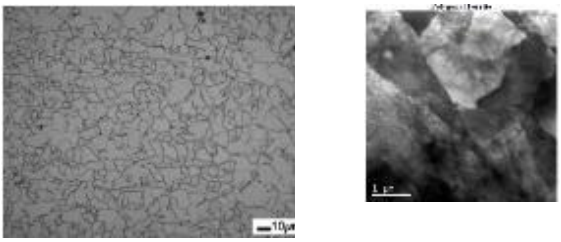

Optical and TEM of Alloy D, predominately polygonal ferrite

Fracture toughness at 800 psi hydrogen pressure

Fracture toughness at 3000 psi hydrogen pressure

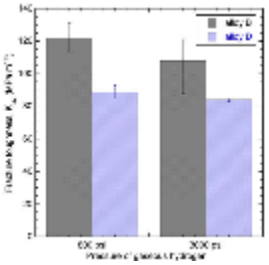

Alloy D fracture toughness at 800/3000 psi hydrogen pressure. Note the stability.

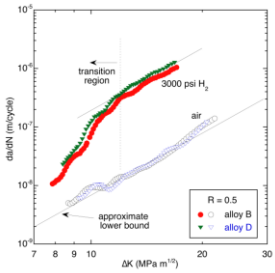

Alloy D fatigue testing in air and 3000 psi hydrogen pressure

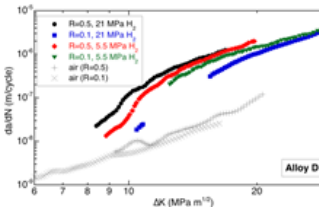

Alloy D fatigue testing in air, 800 and 3000 psi hydrogen pressure

Figure 1: Example of original Alloy D fracture/fatigue performance in high pressure gaseous hydrogen, 800 and 3000 psi.

However, one of the questions that has risen from this testing was while the overall microstructure performed well in fatigue testing what would happen to the fatigue performance if the same alloy design and same predominately pure microstructure of polygonal ferrite had variability in cross-sectional final ferrite grain size homogeneity. This will be the first of several papers that will follow this project

of evaluating fatigue performance in air and hydrogen vs. cross-sectional ferrite grain size homogeneity.

2 MATERIAL AND METHODS

To study the fatigue performance of a common microstructure with different cross-sectional final ferrite grain size homogeneity, laboratory-produced plate trials were developed duplicating the original API X60 HIC Sour Service alloy design but designing the rolling process to create two different cross-sectional final ferrite grain size/homogeneity situations in the laboratory-produced plates. One design utilized a properly optimized, Alloy D1O (Optimized), rolling strategy to generate an optimum Type I Static Recrystallization behavior and Type II No-recrystallization behavior for the niobium content. The second rolling design strategy was a non-optimized, Alloy D2NO (Non-optimized), rolling strategy for Type I Static Recrystallization and Type II No-recrystallization behaviors. A total of 8 laboratory ingots (4-D1O, 4-D2NO) of 100x170x300 mm were rolled into 8 plates 20x180x1300 mm (4-D1O, 4-D2NO). The original "Alloy D" design vs. actual achieved, rolling strategy design vs. actual achieved and original mechanical properties for "Alloy D" vs. the material for the project, Alloy D1O and Alloy D2NO are shown in Tables 1, 2, 2a and 3. Per pass reduction schedules for Alloy D1O and Alloy D2NO are shown in Figure 2.

Table 1: Alloy Design vs. Actual Lab Melt

	C	Mn	Si	Cr	Cu	Ni	Nb
Original Alloy D	.03	1.14	.18	.16	.24	.14	.084
Alloy D1O	.03	1.20	.16	.16	.26	.16	.088
Alloy D2NO	.03	1.16	.15	.15	.26	.15	.084

Table 2: Roughing Rolling Strategy Design vs. Actual Lab Achieved

	Reheat °C	RM FRT °C	RM Total Reduction %	Hold Thickness mm
Design	1180	>1050	D1O-55, D2NO-35	D1O-45, D2NO-65
Alloy D1O	1180	1132	55	45
Alloy D2NO	1180	1115	35	65

Table 2a: Finishing Rolling Strategy Design vs. Actual Lab Achieved

	FMST °C	FM FRT °C	FM Total Reduction %	Start Cool °C	FCT °C	CR °C/s
Design	D1O-880, D2NO-1000	D1O-820-840, D2NO-850-880	D1O-56, D2NO-69	D1O->800, D2NO->800	D1O-650, D2NO-700	3-5
Alloy D1O	864	843	56	822	648	8.7
Alloy D2NO	1004	886	69	856	715	8.8

Table 3: Original vs. Actual Lab Mechanical Properties

	YS MPa (0.2% offset)	TS MPa	El
Original Alloy D	435	486	-
Alloy D1O	520	585	36.5
Alloy D2NO	482	572	31.1

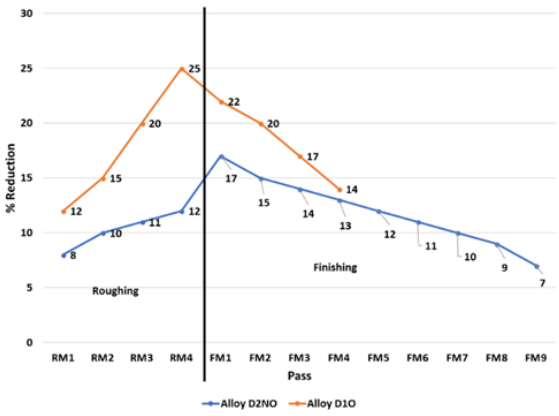

Figure 2: Per pass reduction schedule

Fatigue testing will be performed in the NIST uniquely designed multi sample fatigue testing pressure vessel, Figures 3 and 4.

Figure 3: NIST test vessel for pressurized hydrogen gas

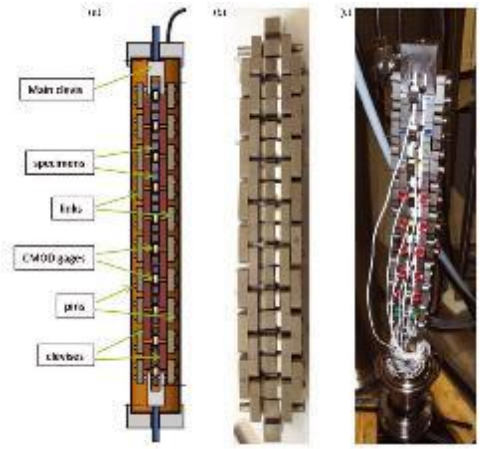

Figure 4: (a) Conceptual drawing showing the elements of the linked chain of specimens, (b) photograph showing the assembled chain with PTFE spacers, and (c) photograph showing the assembled chain, complete with CMOD gages and aluminum spacers ready for installation into the chamber.

Fatigue testing will be done in air and pressurized gaseous hydrogen of 5.5 MPa (800 psi) and 21 MPa (3000 psi) and will be compared to the original Alloy D previously tested. Fatigue testing will be done in accordance with ASTM E647 at load ratios, *R*, of 0.1 and 0.5 [12]. The loading frequency will be 1 Hz, which gives time for hydrogen to diffuse to the crack tip yet is a rate which is fast enough to perform the tests in a reasonable amount of time. The tests will be run in load control, and each specimen will have a CMOD (crack mouth opening displacement) gauge such that crack growth can be determined from compliance. Compact tension (CT) specimens have been machined from the plates of both the D1O and D2NO materials, with the crack oriented in the rolling direction for half of the specimens and perpendicular to the rolling direction for the other half of the specimens. The test chamber has an actuator rod that extends from inside the chamber to outside of the chamber. There are three seals along that length of the actuator rod, and those seals impart load to the actuator rod. Because that load is sometimes inconsistent, an internal load cell is used within the chamber such that no compensation for friction of the seals is required. The specimens have length *W*=45 mm and thickness *B*=19 mm.

3 RESULTS AND DISCUSSION

3.1 – Microstructural Characterization

This “optimized” and “non-optimized” laboratory rolling strategy resulted in distinct differences in the cross-sectional final ferrite grain size and homogeneity. Since strength properties are significantly controlled by low angle grain boundaries (LAGB $4^o<\vartheta<15^o$, D4°) and ductility properties, such as toughness and fatigue, are significantly controlled by high angle grain boundaries (HAGB, $\vartheta > 15^o$, D15°), microstructural characterization of the laboratory-produced plates of both low angle grain boundaries and high angle grain boundaries was performed. The goal of creating similar microstructures in the two laboratory plates with distinctly different cross-sectional final ferrite grain size/homogeneity was realized, Figure 5 [13].

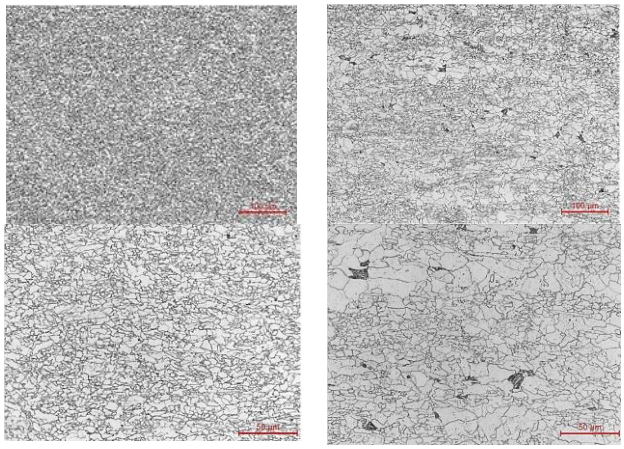

Alloy D1O (Optimized), ¼ thickness, 200x and 500x

Alloy D2NO (Non-optimized), ¼ thickness, 200x and 500x

Figure 5: Example of ¼ thickness microstructure comparison of Alloy D1O (Optimized) vs. Alloy D2NO (Non-optimized)

The microstructure in both the optimized and non-optimized plates was predominately polygonal ferrite with a very small amount of pearlite/bainite seen in the non-optimized plates due to the coarse austinite grain size, Figure 6 [14].

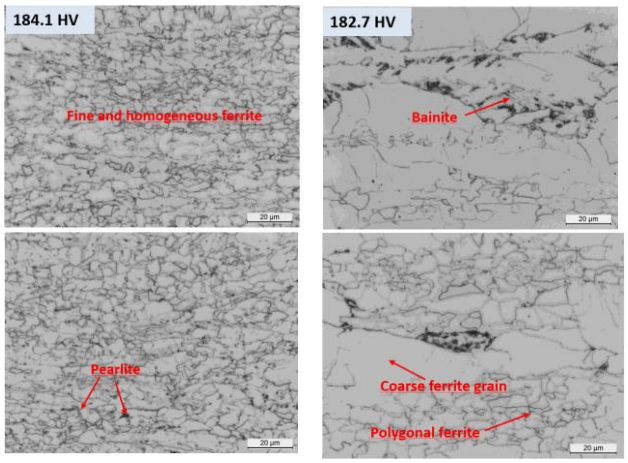

Alloy D1O (Optimized), center thickness

Alloy D2NO (Non-optimized), center thickness

Figure 6: Example comparison of center-thickness microstructure showing predominately polygonal ferrite with very small amounts of pearlite and bainite of Alloy D1O (Optimized) and Alloy D2NO (Non-optimized). Note that bainite was found only in the non-optimized plates.

The optimized plates had an average cross-sectional HAGB ferrite grain size of 3.2 µm with 20% of the cross-sectional average HAGB > 8.5 µm. The non-optimized plates had an average cross-sectional HAGB ferrite grain size of 4.5 µm with 20% of the cross-sectional average HAGB >16.5 µm. For optimum ductility properties average HAGB (finer is better) and the population of larger HAGB representing more than 20% of the accumulated area fraction (finer is better) is the target goal. Detailed microstructural comparisons and grain size distributions can be seen in Figures 7, 8, 9 and 10 and Table 4.

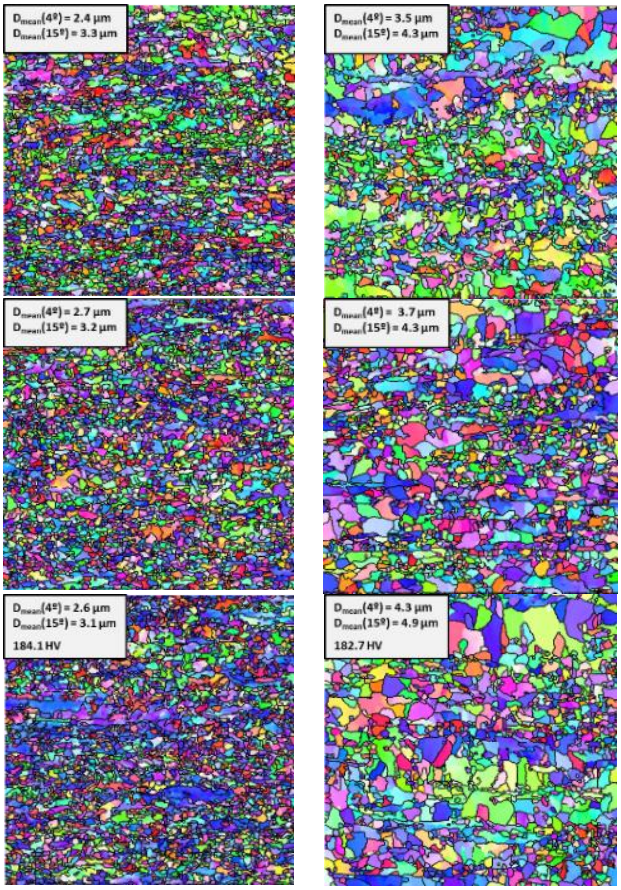

Alloy D1O (Optimized) Top to bottom, Surface, ¼ and center thickness average LAGB/HAGB and microstructure

Alloy D2NO (Non-optimized) Top to bottom, Surface, ¼ and center thickness average LAGB/HAGB and microstructure

Figure 7: EBSD cross-sectional microstructure comparison of Alloy D1O (Optimized) vs. Alloy D2NO (Non-optimized). Note the obvious differences in LAGB/HAGB averages and overall cross-sectional homogeneity.

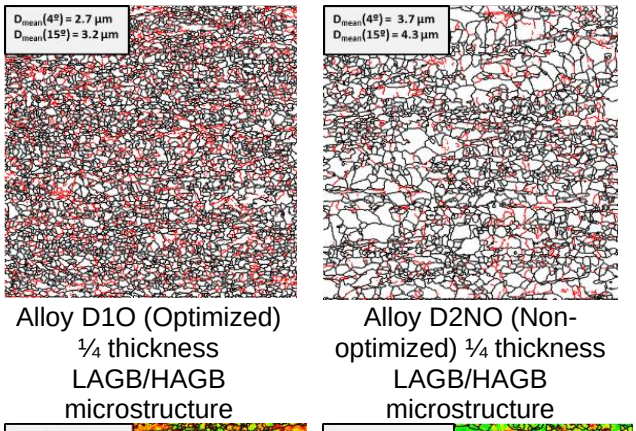

Alloy D1O (Optimized) ¼ thickness LAGB/HAGB microstructure

Alloy D2NO (Non-optimized) ¼ thickness LAGB/HAGB microstructure

Alloy D1O (Optimized) ¼ thickness kernel map

Alloy D2NO (Non-optimized) ¼ thickness kernel map

Figure 8: LAGB/HAGB mapping (top) and kernel mapping (bottom). Kernel mapping shows a slightly higher dislocation density in the Alloy D1O (Optimized).

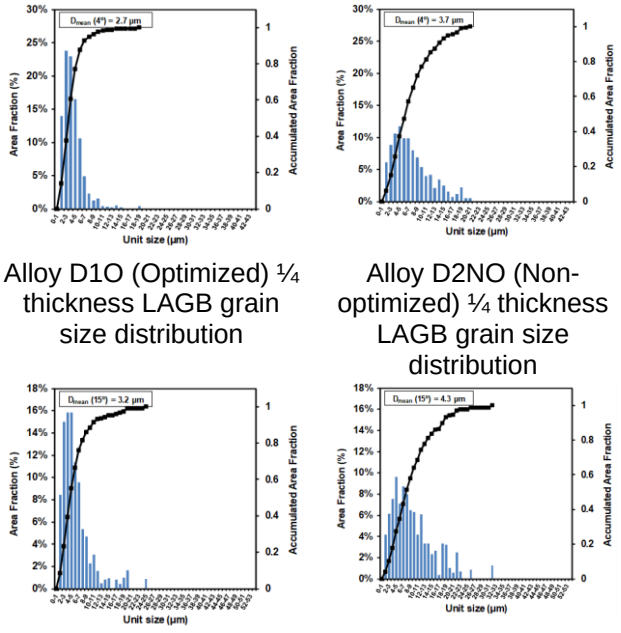

Alloy D1O (Optimized) ¼ thickness LAGB grain size distribution

Alloy D2NO (Non-optimized) ¼ thickness LAGB grain size distribution

Alloy D1O (Optimized) ¼ thickness HAGB grain size distribution

Alloy D2NO (Non-optimized) ¼ thickness HAGB grain size distribution

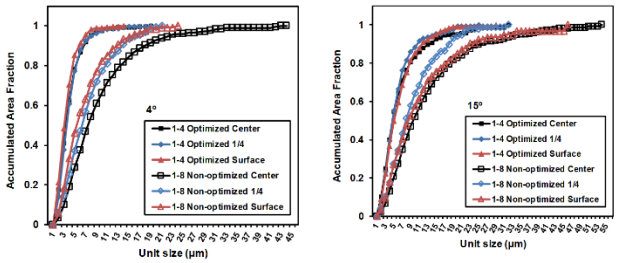

LAGB cross-sectional comparison

HAGB cross-sectional comparison

Figure 9: Surface, ¼ and center thickness LAGB/HAGB cross-sectional comparison

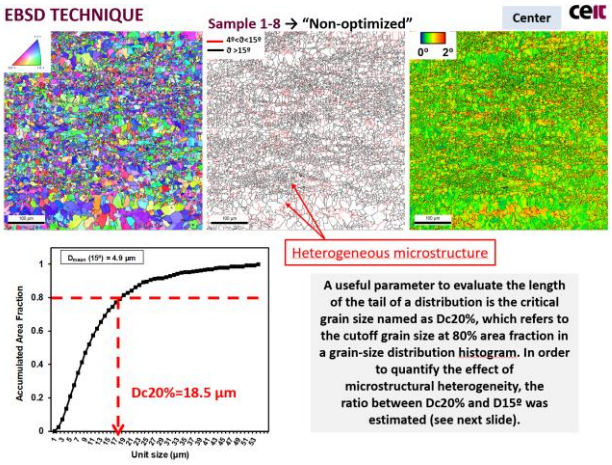

Figure 10: Example of determination of homogeneity HAGB cross-sectional grain size toward ductility properties

Table 4: Analysis of HAGB grain size average and homogeneity of Optimized and Non-optimized plates

		Dc20% (µm)	D15º (µm)	D20%/D15º
Alloy D1O (Optimized)	Center	9.0	3.1	2.9
	¼	7.8	3.2	2.4
	Surface	8.8	3.3	2.6
	Average	8.5	3.2	2.6
Alloy D2NO (Non-optimized)	Center	18.5	4.9	3.8
	¼	13.5	4.9	2.7
	Surface	17.5	4.3	4.1
	Average	16.5	4.7	3.5

3.2 – MicroSim® Austenite Evolution Modeling Results

In addition, modeling of austenite grain size evolution utilizing MicroSim® PM V3 has been done utilizing the processing parameters from the laboratory rolling for comparison with the final observed polygonal microstructure. MicroSim® modeling of the austenite evolution at the

end of the roughing phase and in the finishing phase show that while the averages are relatively similar, there is a large difference in the largest austenite grain (DMax), 90% of the austenite grains below value (DC 0.1) and ZD (cross-sectional homogeneity factor, smaller is more homogenous), Figure 11. In addition, the final austenite grain size distribution prior to accelerated water cooling (ACC) between the optimized and non-optimized rolling shows an obvious difference, Figure 12.

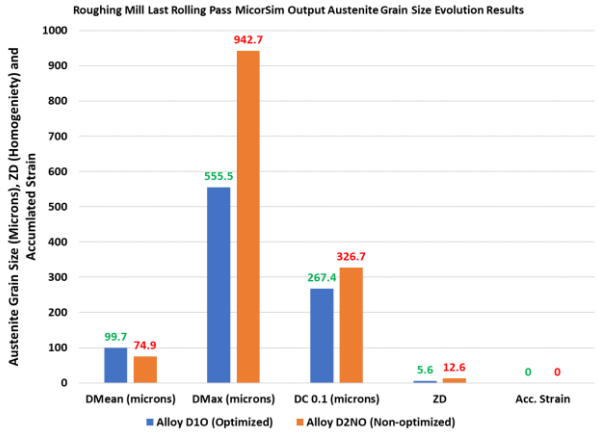

MicroSim® modeling of austenite evolution at the end of the roughing phase of rolling comparison

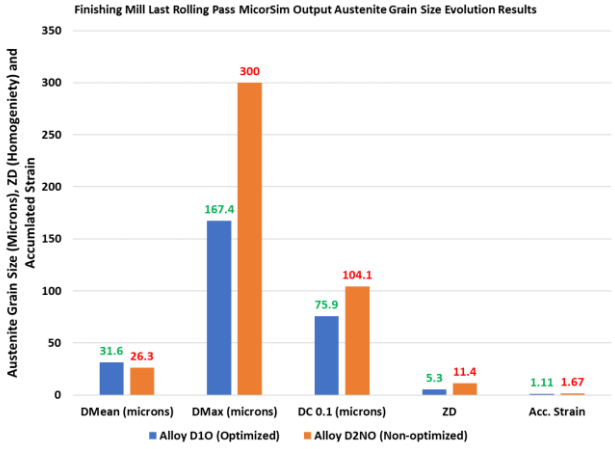

MicroSim® modeling austenite evolution at the end of the finishing phase of rolling comparison

Figure 11: Roughing and Finishing MicroSim® modeling of austenite evolution

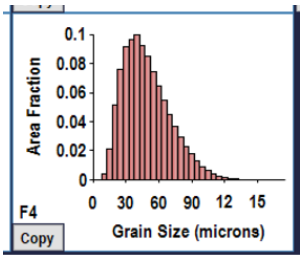

Alloy D1O (Optimized)

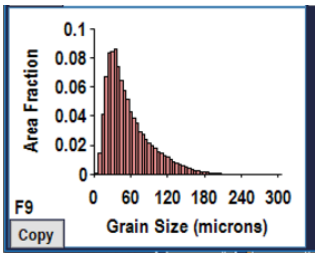

Alloy D2NO (Non-optimized)

Figure 12: Final finishing rolling pass austenite grain size distribution per MicroSim® modeling.

3.3 Charpy Test Results

As a precursor to fatigue testing, Charpy impact testing of the two steels was performed at NIST with temperatures ranging from -196 °C to 21 °C (room temperature). Testing was done in accordance with ASTM E 23 [15]. V-notch specimens 10 mm wide by 10 mm thick by 55 mm long were extracted from the center of the plates with the crack running in the rolling direction and the length of the specimen perpendicular to the rolling direction. The parameters measured were absorbed energy, *KV*, and lateral expansion, *LE*. Ductile-to-brittle transition temperatures (*DBTT*) were obtained from curves of *KV* and *LE* as a function of temperature, shown in Figures 13 and 14, respectively. Upper-shelf energy (*USE*) is calculated from data in Figure 13. Table 5 shows a summary of the results. There is no difference in USE between the steels, but the non-optimized steel is 25 °C more brittle than the optimized steel. The noted USE differences (no difference) is as expected for this very low carbon, lower Mn, low S, inclusion controlled polygonal ferrite microstructure. The ductile-brittle transition temperature (25 °C difference) would be expected due to the differences in HAGB average and heterogeneity through the cross-section.

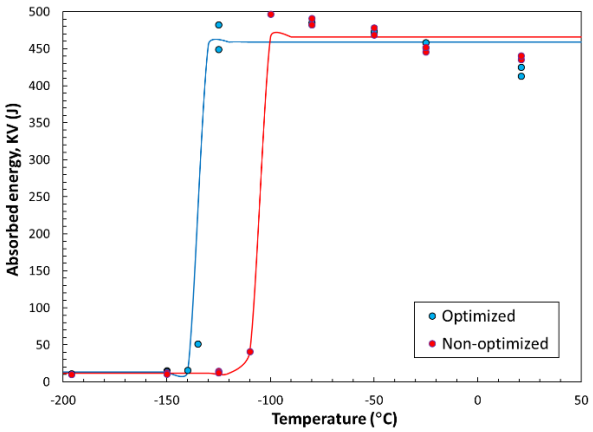

Figure 13: Absorbed energy as a function of temperature for both steels

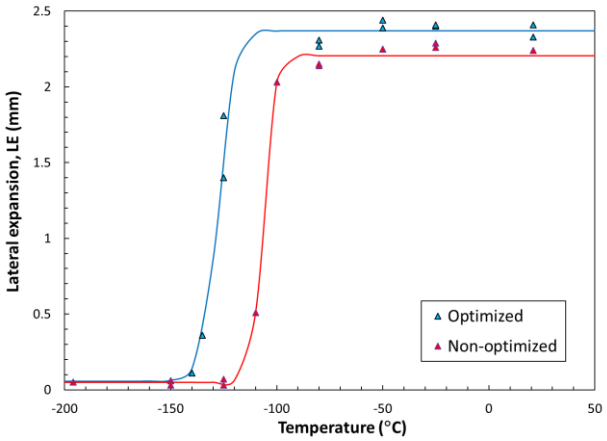

Figure 14: Lateral expansion as a function of temperature for both steels

Table 5: Summary of results of Charpy impact testing of the optimized and non-optimized steels

Material condition	$DBTT_{KV}$ (°C)	USE (J)	$DBTT_{LE}$ (°C)
Optimized	-133	459	-128
Non-optimized	-108	466	-107

Fatigue crack growth rate (FCGR) testing in air, for both the optimized and non-optimized steels, has begun. CT specimens with *W*=45 mm and *B*=19 mm have been machined from the plates. Half of the specimens have T-L orientation and half have L-T orientation, where the first letter designates the loading direction and the second is the direction of crack growth. L is the longitudinal, or plate rolling direction, and T is the direction transverse to the rolling direction. All specimens have cracks extending through the thickness of the plates. All FCGR tests in air will be run at a frequency of 10 Hz and a load ratio (minimum load/maximum load) of 0.5. FCGR tests in hydrogen will be run at a cyclic load frequency of 1 Hz, load ratios of both 0.1 and 0.5, and hydrogen gas pressures of 5.5 MPa (800 psi) and 21 MPa (3000 psi). Both the optimized and non-optimized steels will be tested. Additionally, for this suite of tests on these two steels, fracture toughness tests in air, 5.5 MPa hydrogen gas, and 21 MPa hydrogen gas will be performed.

4 CONCLUSION

A predominately polygonal ferrite microstructure with varying cross-sectional ferrite grain size/distribution has been successfully produced in the laboratory. This will allow for a proper evaluation of the effect of the cross-sectional ferrite grain size/distribution will have on ductility properties such as fatigue performance for a given microstructure in air and high-pressure gaseous hydrogen. Fatigue testing in air is in progress with fatigue testing in high pressure gaseous hydrogen to follow. This paper will be the first of several more on the subject as additional fatigue data is generated from the samples produced. Charpy impact test results show that there is no difference between the USE of the two steels as would be expected from the low carbon, low sulfur polygonal ferrite microstructure produced, but the non-optimized steel is 25 °C more brittle than the optimized steel as would be expected due to the difference in cross-sectional ferrite grain size heterogeneity.

Acknowledgments

Thanks to H2C in Korea for assistance in coordination of the project in Korea. Also, thanks to Hyundai Steel Corporation for their cooperation in producing the laboratory samples.

REFERENCES

1 Lu J, Ivey D, Henein H, Wiskel J, Omotoso O, Microstructure Characterization and Strengthening Mechanisms of Microalloyed Steels, Proceedings of 2008 ASME International Pipeline Conference, Calgary, Canada, September 2008.

2 Barbosa R, Rodriguez-Ibabe JM, Stalheim D, Rebellato M, Alloy Cost Optimization Through Proper Metallurgical Development of Strength and Ductility Properties in Structural Steels, Proceedings of AISTech 2018, Philadelphia, PA, USA, 2018.

3 Stalheim D, Generation of Stable Optimized Thru-thickness Mechanical Properties in Wide Heavy Gauge Structural Steel Plate, Proceedings of AISTech 2018, Philadelphia, PA, USA, 2018.

4 Isasti N, Jorge-Badiola D, Taheri ML, Uranga P, Microstructural Features Controlling Mechanical Properties in Nb-Mo Microalloyed Steels Part II: Impact Toughness, Metallurgical. Material Transaction A, Vol. 45A, 2014, pp. 4972-4982.

5 ASME B31.12-2014, Hydrogen Piping and Pipelines, American Society of Mechanical Engineers, New York, NY, 2014.

6 Drexler ES, McColskey JD, Slifka AJ, et al., Apparatus for Accelerating Measurements of Environmentally Assisted Fatigue Crack Growth at Low Frequency, Society for Experimental Mechanisms, 2014.

7 Stalheim D, Materials Solutions for Hydrogen Delivery in Pipelines, 2011 US DOE Hydrogen Program Annual Merit Review and Peer Evaluation Meeting, Arlington, VA, USA, 2011.

8 Stalheim D, Final Report on Fracture Toughness Testing in Gaseous Hydrogen – Phase 1, Internal report to ASME ST-LLC, January 2011.

9 Stalheim D, Boggess T, San Marchi, C, Somerday B, Govindarajan M, Sofronis P, et al., Microstructure and Mechanical Property Performance of Commercial Grade API Pipeline Steels in High Pressure Gaseous Hydrogen, Proceedings ASME 8th International Pipeline Conference, Calgary, Canada, 2010.

10 Stalheim DG, Boggess T, Bromley D, et al., Continued Microstructure and Mechanical Property Performance Evaluation of Commercial Grade API Pipeline Steels in High Pressure Gaseous Hydrogen, Proceedings ASME 9th International Pipeline Conference, Calgary, Canada, 2012.

11 San Marchi C, Somerday B, Nibur K, Stalheim D, Fracture and Fatigue of Commercial Grade API Pipeline Steels in Gaseous Hydrogen, Proceedings of ASME 2010 Pressure Vessels and Piping Division/K-PVP Conference, Bellevue, WA, USA, 2010.

12 ASTM Standard E 647-11 "Test Method for Measurement of Fatigue Crack Growth Rates". 2011, ASTM International.

13 Kang DH, HSC RD Lab Test Results Related to H2 Infrastructure Development, Hyundai Steel Corporation, Internal Project Correspondence, January 2019.

14 Uranga P, Ibabe-Rodriguez JM, Isasiti N, Azpeitia X, High Pressure Gaseous Hydrogen Pipe, CEIT, Internal Project Correspondence, February 2019.

15 ASTM Standard E 23-18 "Standard Test Methods for Notched Bar Impact Testing of Metallic Materials". 2018, ASTM International.